J. Fluid Mech. (1972), *vol.* 52, *part* 4, *pp.* 639–656
Printed in Great Britain

The tearing of an adhesive layer between flexible tapes pulled apart

By A. S. WILLIAMSON

Koninklijke/Shell Exploratie en Produktie Laboratorium,
Rijswijk, Holland

(Received 21 July 1971)

The tearing of a pressure-sensitive ('tacky') adhesive is examined. Two flexible strips bonded by a layer of adhesive are passed between adjacent cylindrical guides and peeled apart, causing the adhesive layer to separate into two about a surface tension membrane. Treating the adhesive as a Newtonian viscous fluid, the slow-flow problem is solved by an iterative numerical scheme in which the surface tension membrane boundary in the vicinity of the region of separation is approximated by a shear-free boundary given by a sixth-degree polynomial expression. The energy dissipation rate, a measure of the 'strength' of the adhesive, is obtained from the flow.

The solution method is also used to determine the similar flow induced by two counter-rotating rollers partially immersed in a large bath of fluid. The results are in fairly good agreement with available experimental data. The symmetrical eddies observed under the lowest point of the surface tension membrane in the stable flow between the rollers are reproduced in the solution, proving that fluid inertia effects are not essential for their existence.

1. Introduction

The phenomenon of 'stickiness' in pressure-sensitive (tacky) adhesives has been explained in terms of viscous fluid behaviour (e.g. Bickerman 1968). In considering the failure of such an adhesive it therefore seems natural to investigate the corresponding viscous fluid flow. In this paper the steady-state peeling separation of two flexible strips (tapes) bonded by a viscous fluid layer as they are torn apart is examined (see figure 1). The strips are separated by pulling them around two adjacent frictionless cylindrical guides.

The related flow which occurs in the adhesive layer between a peeling tape and a plane was investigated by McEwan & Taylor (1966). Their solution, re lating the angle at which the tape peels off the plane to the tape tension and the speed of advance of peeling, involved the use of empirical data and did not permit the determination of the detailed flow in the separation region. Pitts & Greiller (1961) examined, both theoretically and experimentally, the flow induced by two rollers partially immersed in a bath of viscous fluid and counter-rotated to draw fluid up through the narrow gap between them. Above the gap,

the fluid separated under a surface tension membrane into two films† which travelled around with the rollers and returned to the bath. In the section of the paper dealing with the two-dimensional flow of this system the analytical treatment was approximate and confined to the neighbourhood of the lowest point of the surface tension membrane.

2. The peeling model

The flow considered is the plane, steady, slow (i.e. inertialess) flow of an incompressible viscous fluid. Gravity effects other than a uniform atmospheric pressure are omitted, as Pitts & Greiller found them to be negligible in the cases of interest. The possibility of cavitation effects (see Banks & Mills 1954) is not considered and the flow is taken to be symmetrical about the x axis in figure 1.

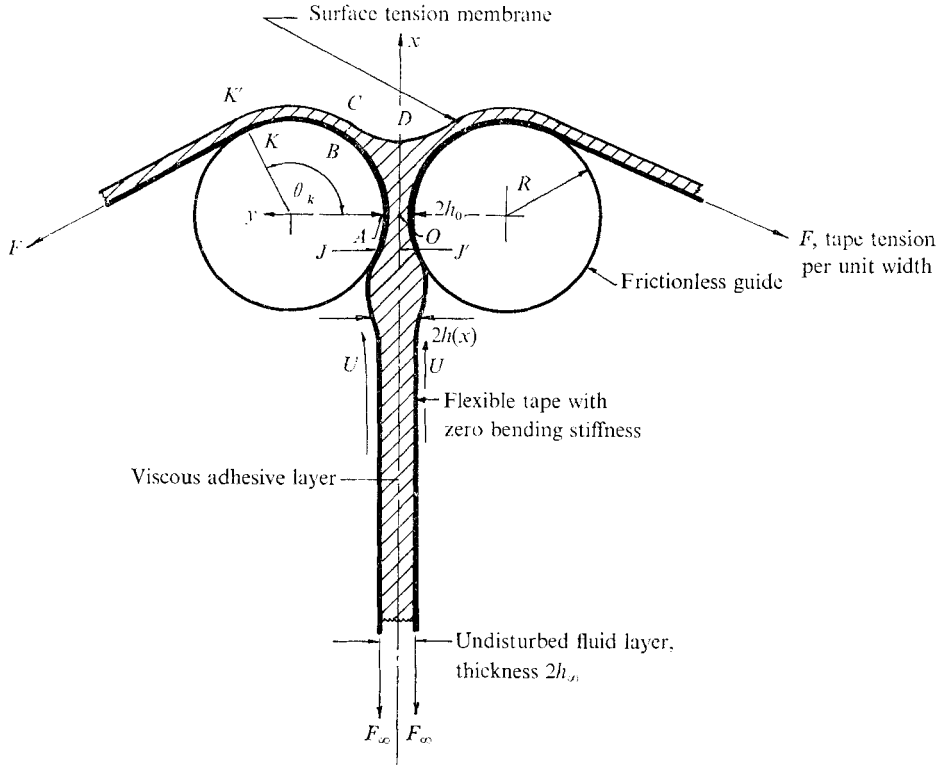

FIGURE 1. The peeling flow.

The tapes are inextensible and have no bending rigidity, the tape tension is F, and the tape speed is U, a constant. Far below the guides it is tentatively assumed that the tapes and fluid layer can be in an undisturbed state, moving as a rigid body (the assumption is subsequently confirmed). In this region the tape tension

† The word 'film' is reserved for a thin fluid layer. At a fluid–air interface the skin, of molecular thickness, which behaves as if under tension is called a surface tension membrane.

is F_∞ and the fluid layer thickness is $2h_\infty$. The values of the following parameters are considered given:

$$\mu U/T, \quad h_0/R, \quad h_\infty/R, \quad F_\infty/T, \tag{2.1}$$

where T is the surface tension, μ is the coefficient of viscosity and $2h_0$ is the closest approach of the guides (at the 'nip' section in figure 1), which are of radius R. A method is developed for determining the resulting flow when (i) $h_0/R \ll 1$, (ii) the fluid layer thickness before tape contact with the guides is approximately $2h_\infty$. Since the boundary conditions on the flow alter as the tapes pass through the guides, different flow regions are treated separately in the analysis and continuity conditions are used to relate neighbouring flows at junctions.

2.1. *The flow between the tapes prior to contact with the guides*

By confining attention to cases where the tape slope and curvature are small the flow may be obtained from the Reynolds approximation. The boundary conditions are taken as

$$(du/dy)_{y=0} = 0, \quad u(x,h) = U. \tag{2.2}$$

The Reynolds flow equation leads to

$$u = U[1 + (3/2h^3)(h_\infty - h)(h^2 - y^2)], \tag{2.3}$$

$$dp/dx = (3\mu U/h^3)(h - h_\infty). \tag{2.4}$$

For small tape slopes equilibrium requires

$$dF/dx = \tau_{xy}(x,h) = (3\mu U/h^2)(h - h_\infty), \tag{2.5}$$

where τ_{xy} is the shear stress on the fluid, and

$$F(d^2h/dx^2) = -p. \tag{2.6}$$

Equations (2.4) and (2.6) are similar to those used by McEwan & Taylor. In (2.5) the variation of tape tension is included but for the cases considered in this paper (in which $|h - h_\infty|/h_\infty \ll 1$) it will be seen that this variation is negligible.

No general closed-form solution for $h(x)$ has been found. The equations may be linearized about the solution

$$h = h_\infty, \quad F = F_\infty, \quad p = 0.$$

Letting

$$F = F_\infty(1 + F'), \quad h = h_\infty(1 + h'), \quad \alpha^3 = 3\mu U/8F_\infty \tag{2.7}$$

and neglecting second-order terms in F' and h', the solution for h' may be written as

$$h' = A\exp(-2\alpha x/h_\infty) + B\exp(\alpha x/h_\infty)\sin(\sqrt{3}\alpha x/h_\infty + \epsilon). \tag{2.8}$$

Equation (2.8) is similar to McEwan & Taylor's result. For consistency with the assumption $\lim_{x\to-\infty} h = h_\infty$, $A = 0$. Constants B and ϵ, and the location of the first contact of tape and guide, section JJ' (see figure 1), are found by matching the flows in the regions adjoining JJ'. At the junction the fluid-layer thickness and pressure must be continuous, and since a discontinuity in tape slope would require the guide to exert a tensile load on the tape, the tape slope must be continuous.

2.2. *Reynolds flow when the tapes are in contact with the guides*

The spreading of the flow beneath the surface tension membrane necessitates the full biharmonic treatment in that region. Below the nip section, however, the assumptions of Reynolds flow are satisfied providing that

$$h/R \ll 1 \quad \text{and} \quad |dh/dx| \ll 1. \tag{2.9}$$

In the (x, y) co-ordinate system (see figure 1) the left-hand guide surface in the neighbourhood of the nip is given by

$$h = h_0 + x^2/2R. \tag{2.10}$$

The flow equation leads to (2.4), where h is known from (2.10). To integrate (2.4) it is convenient to introduce the new variables λ and ϕ defined by

$$q = \lambda U h_0, \tag{2.11}$$

where q is the flow rate, and

$$x = (2Rh_0)^{\frac{1}{2}} \tan\phi, \quad |\phi| < \tfrac{1}{2}\pi. \tag{2.12}$$

Integration introduces one constant. Supposing, for the present, that at section OA p is known, $p = p_0$ say, then

$$\frac{h_0(p-p_0)}{3\mu U}\left(\frac{h_0}{2R}\right)^{\frac{1}{2}} = \tfrac{1}{2}\phi + \tfrac{1}{4}\sin 2\phi - \lambda\,(\tfrac{3}{8}\phi + \tfrac{1}{4}\sin 2\phi + \tfrac{1}{32}\sin 4\phi). \tag{2.13}$$

2.3. *Reynolds flow between the surface tension membrane and the tape after separation has occurred*

Far downstream from the membrane vertex point D the flow approaches a uniform state and may be determined from the Reynolds approximation. It is convenient here to consider the flow shown in figure 2. A film thickness $w(x)$ is bounded by a rigid plane translating with velocity U and a steady membrane of surface tension T.

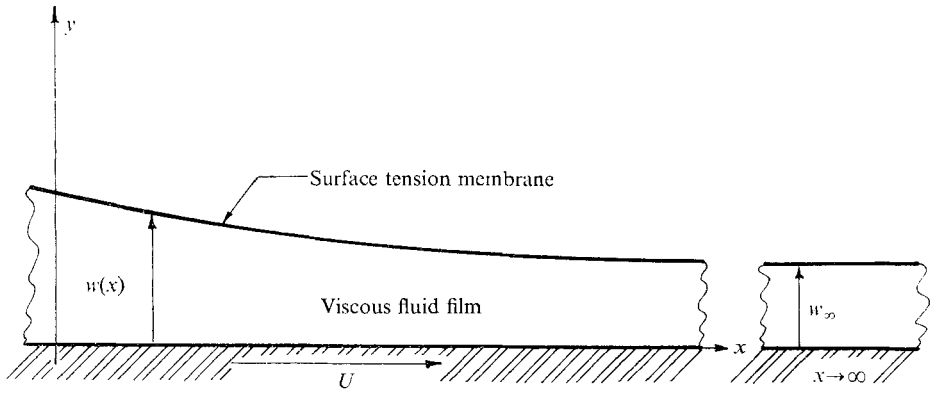

FIGURE 2. Steady-state film of varying thickness between a surface tension membrane and a translating plane.

At the membrane there are generally three conditions on the flow:

$$\psi = \text{constant}, \tag{2.14}$$

$$\tau_{ns} = 0, \tag{2.15}$$

$$\sigma_n = T\kappa, \tag{2.16}$$

where ψ is the stream function, τ_{ns} and σ_n are the shear and normal stress components, and κ is the membrane curvature. For the Reynolds approximation to be valid

$$|w\kappa| \ll 1 \quad \text{and} \quad |dw/dx| \ll 1; \tag{2.17}$$

then the following approximations may be made:

$$\tau_{ns} = \tau_{xy}, \quad \sigma_n = \sigma_y, \quad \kappa = d^2w/dx^2.$$

Substituting in (2.15) and (2.16), these lead to

$$(du/dy)_{y=w} = 0, \tag{2.18}$$

$$\sigma_y(x, w) = Td^2w/dx^2. \tag{2.19}$$

Condition (2.14) is automatically satisfied by the Reynolds flow postulates. At the lower boundary

$$u(x, 0) = U. \tag{2.20}$$

The flow equation yields $dp/dx = (3/w^3)(Uw - q)$, (2.21)

$$u = U + 3(U/w^2 - q/w^3)(\tfrac{1}{2}y^2 - wy), \tag{2.22}$$

where q is the flow rate. From the stress strain-rate relation for a viscous fluid

$$\sigma_y = -p + 2\mu\dot{\epsilon}_y, \tag{2.23}$$

$$\dot{\epsilon}_y(x, w) = -(\partial u/\partial x)_{y=w}. \tag{2.24}$$

Equation (2.22) is obtained under the assumption that

$$|\partial u/\partial x| \ll |\partial u/\partial y|.$$

Having thus found u, the derivative with respect to x may legitimately be taken although, for consistency, it should always be dropped in comparison to the y derivative. From (2.24), therefore,

$$\dot{\epsilon}_y(x, w) = \frac{3q}{2w^2}\frac{dw}{dx} \tag{2.25}$$

and substitution into (2.19) gives

$$T\frac{d^3w}{dx^3} - 3\mu q\frac{d}{dx}\left(\frac{1}{w^2}\frac{dw}{dx}\right) + \frac{3\mu U}{w^3}\left(w - \frac{q}{U}\right) = 0. \tag{2.26}$$

The above analysis is similar to the treatment by Bretherton (1961) of the thickness variation of thin films in tubes. Here, however, the strain-rate term in equation (2.26), the second term, is seen to be of magnitude comparable with that of the other terms and is not omitted.

No general solution to (2.26) has been found. As in the treatment of the flow in § 2.1, a linearized solution may be obtained about the solution

$$w = w_\infty = q/U$$

by setting $\quad w = w_\infty(1+w'), \quad \xi = x/w_\infty, \quad \beta = 3\mu U/T.$

Substitution into (2.26) and omission of all but linear terms in w' yields

$$d^3w'/d\xi^3 - \beta(d^2w'/d\xi^2) + \beta w' = 0. \tag{2.27}$$

Equation (2.27) has solutions of the form

$$w' = Ce^{a\xi}, \tag{2.28}$$

where C is a real coefficient and a satisfies

$$a^3 - \beta a^2 + \beta = 0. \tag{2.29}$$

For $\lim_{x\to\infty} w' = 0$, it follows that

$$Re\,(a) < 0. \tag{2.30}$$

From the relations between the roots of a cubic polynomial it can readily be proved that there is only one admissible root and that it is real. Thus

$$w = w_\infty(1+Ce^{a\xi}) \tag{2.31}$$

and the film approaches the uniform state with either monotonically increasing or decreasing thickness according as C is positive or negative.

These results may be applied when the translating surface is circular, with radius R, providing that $w/R \ll 1$. This restriction is satisfied when the restrictions specified in § 2.1 are satisfied and h_∞/h_0 is of order unity. At section KK' in figure 1 the tapes depart tangentially from the guides, otherwise the resulting tape slope discontinuity would require the guide to exert a tensile line load. Any variation in the film thickness caused by the sudden change in tape curvature as it leaves the guide is assumed to be sufficiently small to have no influence on the flow in the tearing region. In terms of the polar co-ordinates (r, θ), with origin at the centre of the left-hand guide in figure 1,

$$p = (3\mu U/2aw_\infty)\{1-[1+C\exp(aR\theta/w_\infty)]^{-2}\} + T/R. \tag{2.32}$$

As the film approaches the rigid coating state, p approaches T/R.

2.4. *Flow in the separation region*

In the region shown as $OABCD$ in figure 1 the configuration of the surface tension membrane boundary, and therefore the energy dissipation rate within the fluid, is dependent on the flow. Because of the analytical difficulties of biharmonic free-boundary flows, the solution is obtained by a finite-difference numerical method described in § 3. In the solution, CD is considered to be a shear-free boundary, thus satisfying conditions (2.14) and (2.15), with position prescribed by a sixth-degree polynomial. Such a boundary may be thought of as a surface tension membrane with a supplementary normal stress S, forcing the membrane to adopt the curve given by the polynomial. The polynomial coefficients are then adjusted to satisfy (2.16) as closely as possible.

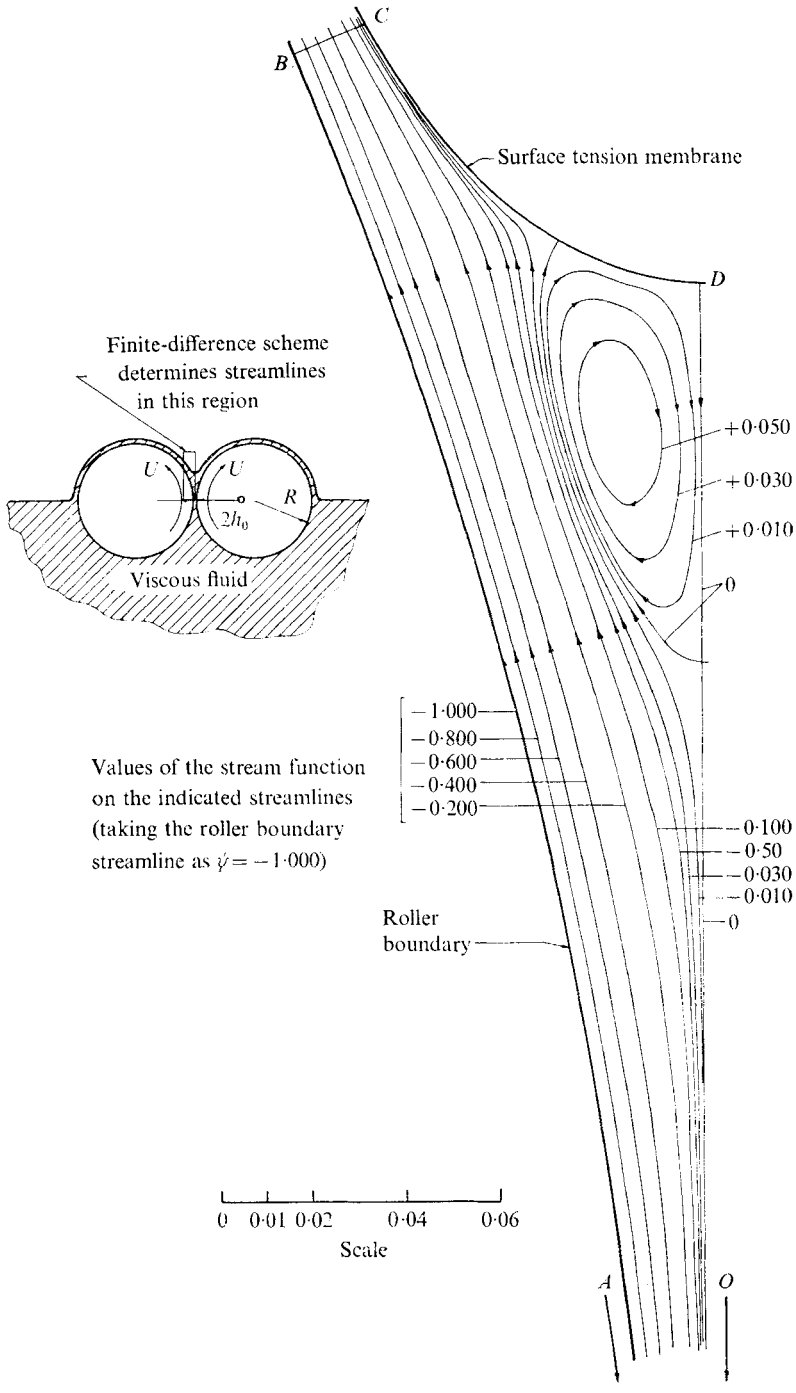

FIGURE 3. Streamline pattern in the region of the numerical solution *OABCD* for $h_0/R = 0{\cdot}01$, $\mu U/T = 0{\cdot}1$, $h_\infty/h_0 = 1{\cdot}380$. (The insert refers to §3.)

At BC the film thickness w_c is taken as the arbitrarily decided maximum at which the results of §2.3 are applicable. In the examples presented here the ratio $w_c/w_\infty = 1{\cdot}20$ was used. The slope and curvature of the boundary are taken to be continuous at point C and these two conditions ensure that S is zero at the junction point. In terms of the dimensionless co-ordinates

$$X = x/R, \quad Y = y/R$$

the curve CD is represented by

$$X = b_0 + b_1 Y^2 + b_2 Y^4 + b_3 Y^6.$$

The determination of the four coefficients b_i requires two additional conditions. It was found to be convenient to specify the angle θ_c and the position of point D, X_D. The quantities X_D and θ_c are referred to as the adjustable parameters of CD. Now

$$X_c = (1 + w_c/R)\sin\theta_c,$$

$$Y_c = (1 + h_0/R) - (1 + w_c/R)\cos\theta_c,$$

so the equations governing b_i are:

$$b_0 = X_D, \quad b_1 Y_c^2 + b_2 Y_c^4 + b_3 Y_c^6 = X_c - b_0,$$

$$2b_1 Y_c + 4b_2 Y_c^3 + 6b_3 Y_c^5 = \cot[\theta_c - a(w_c/w_\infty - 1)].$$

Since the curvature and slope are continuous at C, d^2X/dY^2 is also continuous at C. Approximately,†

$$\frac{d^2X}{dY^2} = R\left[\frac{1}{R^2}\frac{d^2w}{d\theta^2} - \frac{1}{R}\right]\left[1 + \left(\frac{dX}{dY}\right)^2\right]_c^{\frac{3}{2}},$$

which leads to $$2b_1 + 12b_2 Y_c^2 + 30b_3 Y_c^4 = \frac{a^2 R(w_c - w_\infty)/w_\infty^2 - 1}{\sin^3[\theta_c - a(w_c/w_\infty - 1)]}.$$

The boundary conditions on the flow are:

(i) On DO, from symmetry, $\psi = 0$, $\nabla^2\psi = 0$.

(ii) On OA, ψ and $\nabla^2\psi$ are known from §2.2.

(iii) On AB, $\psi = -Uh_\infty$, $\partial\psi/\partial r = U$.

(iv) On BC, ψ and $\nabla^2\psi$ are known from §2.3.

(v) On CD, $\psi = 0$, $\tau_{ns} = 0$.

To determine a trial flow, numerical values are assigned to the parameters in (2.1). Initial values are selected for b_0 and θ_c from a scale drawing of a plausible flow. With the finite-difference scheme outlined in §3 the stream function, in the dimensionless form ψ/Uh_0, is determined numerically at each mesh node. From this solution the normal stress ratio $\sigma_n R^2/\mu U h_0$ is determined at each mesh node lying on boundary CD except for a constant. The constant is evaluated from the pressure at C known from (2.32). The supplementary stress ratio is then found:

$$\frac{SR^2}{\mu U h_0} = \frac{T\kappa R^2}{\mu U h_0} - \frac{\sigma_n R^2}{\mu U h_0}. \tag{2.33}$$

† See for example, Lamb (1932, p. 178).

The quantity e,

$$e = S/T\kappa, \tag{2.34}$$

is a measure of the relative magnitude of S compared to the membrane stress $T\kappa$. The average and root-mean-square values of e are calculated. Depending on the size and distribution of e an adjustment is made to either b_0 or θ_c. With the new values of b_0 and θ_c another solution is commenced. This process is repeated

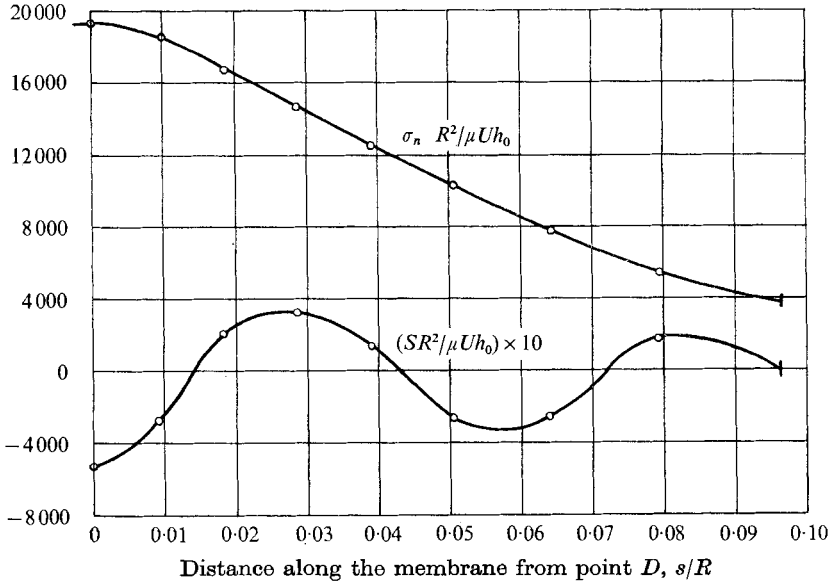

FIGURE 4. The variation of σ_n, the normal stress on CD, and S along the shear-free boundary in the flow of figure 3. Average fractional error e_a in $S/T\kappa$ is $-0{\cdot}00348$, root-mean-square fractional error $e_r = 0{\cdot}0249$. Polynomial representation of curve CD with $b_0 = 0{\cdot}3345$, $\theta_c = 0{\cdot}3950$ given by

$$x/R = 0{\cdot}3345 + 9{\cdot}3110\,(y/R)^2 + 393{\cdot}1013\,(y/R)^4 - 11837{\cdot}87\,(y/R)^6.$$

	Optimal values	Variations in b_0		Variations in θ_c	
b_0	0·3345	0·3340	0·3350	0·3345	0·3345
Change in b_0 from optimal	—	−0·15 %	+0·15 %	0	0
θ_c	0·3950	0·3950	0·3950	0·3945	0·3955
Change in θ_c from optimal	—	0	0	0·13 %	+0·13 %
e_r	0·02499	0·03790	0·03660	0·03127	0·02987
Change in e_r	—	+51·96 %	+46·7 %	+25·2 %	+19·6 %

TABLE 1. Sensitivity of e_r to small perturbations of b_0 and θ_c from the optimal values for the flow in figure 3

until e is reduced to satisfactory levels. With a sixth-degree polynomial representation of CD there was little difficulty in the case examined here in meeting the requirements

$$|e_a| < 0{\cdot}01, \quad e_r < 0{\cdot}03,$$

after approximately ten iterations, where e_a and e_r are the average and r.m.s. values of e respectively. The sensitivity of e_r at these values to perturbations in

b_0 and θ_c for the flow of figure 3 is shown in table 1. This may be summarized by observing that a $\frac{1}{6}\%$ change in b_0 increases e_r by approximately 45%, and a $\frac{1}{8}\%$ change in θ_c increases e_r by approximately 20%.

2.5. *The complete flow*

The complete flow is obtained by combining the flows of §§2.2, 2.3, and 2.4. Between KK' and BC the flow is known from the results of §2.3. At BC the choice of boundary conditions there assures the continuity of flow. In $OABCD$ the flow is determined numerically and the value of p_0 obtained from the solution. The location of section JJ', the junction of the tapes and guides, is found from application of the continuity conditions of §2.1. These lead to

$$B\exp\left(\frac{\alpha x_J}{h_\infty}\right)\sin\Lambda = \frac{h_0}{h_\infty}+\frac{x_J^2}{2Rh_\infty}-1, \tag{2.35}$$

$$B\exp\left(\frac{\alpha x_J}{h_\infty}\right)[\sin\Lambda+3^{\frac{1}{2}}\cos\Lambda] = \frac{x_J}{\alpha R}, \tag{2.36}$$

$$\begin{aligned} B\exp\left(\frac{\alpha x_J}{h_\infty}\right)&[\sin\Lambda-3^{\frac{1}{2}}\cos\Lambda] \\ &= \frac{1}{2\alpha^2}\frac{T}{F_\infty}\left\{\frac{p_0h_\infty}{T}+\frac{3\mu U}{T}\frac{h_\infty}{h_0}\left(\frac{2R}{h_0}\right)^{\frac{1}{2}}\right. \\ &\quad\left.\times\left[\tfrac{1}{2}\phi_J+\tfrac{1}{4}\sin 2\phi_J-\frac{h_\infty}{h_0}(\tfrac{3}{8}\phi_J+\tfrac{1}{4}\sin 2\phi_J+\tfrac{1}{32}\sin 4\phi_J)\right]\right\}, \end{aligned} \tag{2.37}$$

where

$$\Lambda = 3^{\frac{1}{2}}\alpha x_J/h_\infty+\epsilon$$

and ϕ_J is the value of ϕ at section JJ'. These equations are to be solved for B, ϵ and x_J/R (or ϕ_J), given the quantities in (2.1). However, it is more convenient to prescribe x_J/R (or ϕ_J) and solve for B, ϵ, and F_∞/T. By obtaining the solution for several suitable values of x_J/R the original problem may be solved by interpolation. The equations are first solved for F_∞/T (or α, see (2.7)). Adding (2.36) and (2.37) and combining with (2.35), a quadratic equation in α is obtained, the solution of which is

$$\alpha = \frac{h_0/h_\infty+x_J^2/2Rh_\infty-1}{4LT/3\mu U}\pm\left[\left(\frac{h_0/h_\infty+x_J^2/2Rh_\infty-1}{4LT/3\mu U}\right)^2-\frac{x_J/R}{LT/3\mu U}\right]^{\frac{1}{2}}, \tag{2.38}$$

where

$$L = \frac{p_0h_\infty}{T}+\frac{3\mu U}{T}\frac{h_\infty}{h_0}\left(\frac{2R}{h_0}\right)^{\frac{1}{2}}\left[\tfrac{1}{2}\phi_J+\tfrac{1}{4}\sin 2\phi_J-\frac{h_\infty}{h_0}(\tfrac{3}{8}\phi_J+\tfrac{1}{4}\sin 2\phi_J+\tfrac{1}{32}\sin 4\phi_J)\right].$$

The requirement $\alpha > 0$ is used to select the appropriate root. In those cases for which $x_J/R \to 0$,

$$\alpha = \frac{2x_J/R}{h_0/h_\infty-1}$$

and

$$\frac{F_\infty}{T} = \frac{3}{64}\frac{\mu U}{T}\left(\frac{h_0/h_\infty-1}{x_J/R}\right)^3. \tag{2.39}$$

It is interesting to note that for finite values of F_∞/T, section JJ' will not coincide with OA. This condition, together with the continuity of tape slope at section JJ' and the tape form, (2.8), below JJ' requires the adhesive layer to 'bulge' slightly before the tapes touch the guides. The values of B and ϵ are now readily obtained. Figure 5 shows a specimen curve of the variation of x_J/R with F_∞/T when the other parameters of (2.1) take the values indicated.

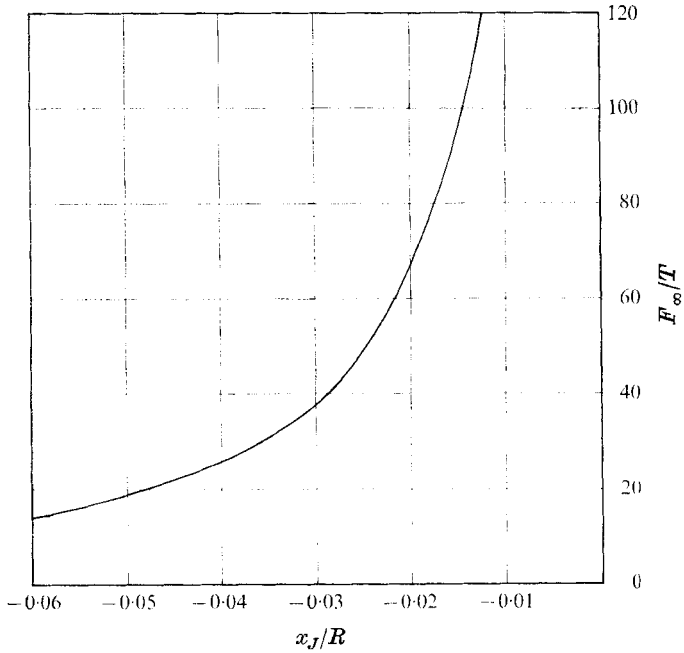

FIGURE 5. The variation of x_J/R with F_∞/T for the linearized tape form solution of §2.1 with $\mu U/T = 0{\cdot}1$, $h_\infty/h_0 = 1{\cdot}38$, $h_0/R = 0{\cdot}01$.

The energy dissipation rate $\dot{W}$ is

$$\dot{W} = 2(F_K - F_\infty)\, U + 2UT.$$

Below JJ' and above BC, where linearized solutions have been used for the flow, the variation in tape tension is negligible compared with the variation between JJ' and BC. Accordingly

$$\dot{W}/UT = 2\,(F_B/T - F_J/T) + 2.$$

Between JJ' and OA, in figure 1, the tape tension variation is obtained from (2.5); above the nip the variation is determined from the numerical solution. For the flow of figure 3, taking $F_\infty/T = 60$, the tension variation is shown in figure 6, and

$$\dot{W}/UT = 4{\cdot}674. \tag{2.40}$$

Since the value of F_∞/T can be chosen arbitrarily it is necessary to check that there is positive pressure between the guide and tape, i.e.

$$F/T > -pR/T. \tag{2.41}$$

In figure 6 it is evident that (2.41) is satisfied.

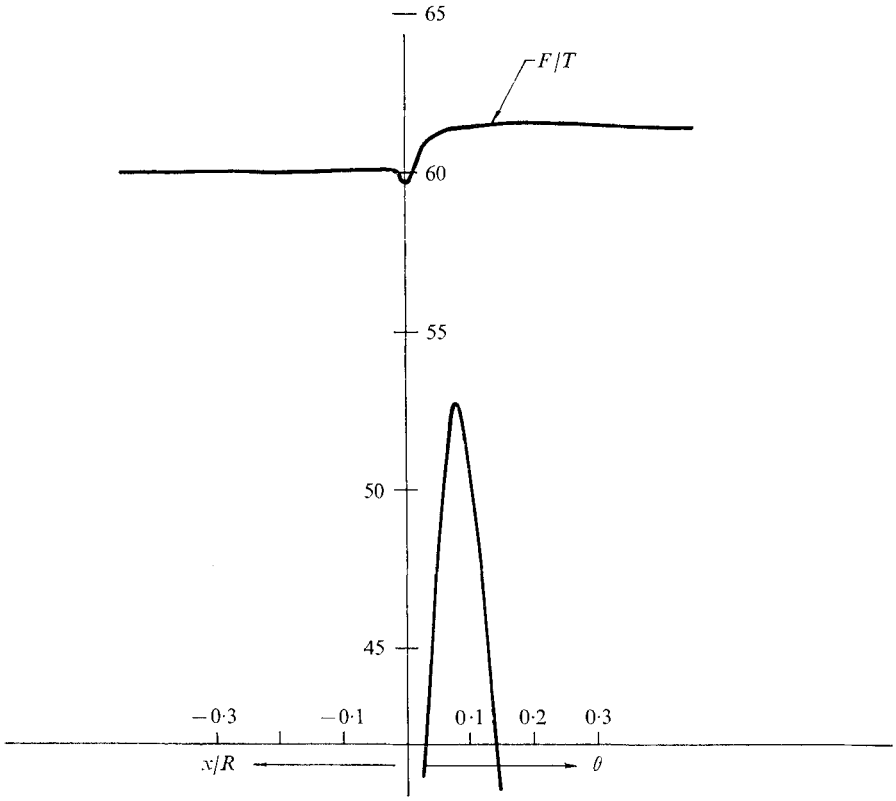

FIGURE 6. The variation of the tape tension ratio F/T for the flow: $\mu U/T = 0{\cdot}1$, $h_\infty/h_0 = 1{\cdot}38$, $h_0/R = 0{\cdot}01$, $F_\infty/T = 60{\cdot}0$. Also shown is the curve of $-pR/T$, to confirm that there is positive pressure between the guide and tape.

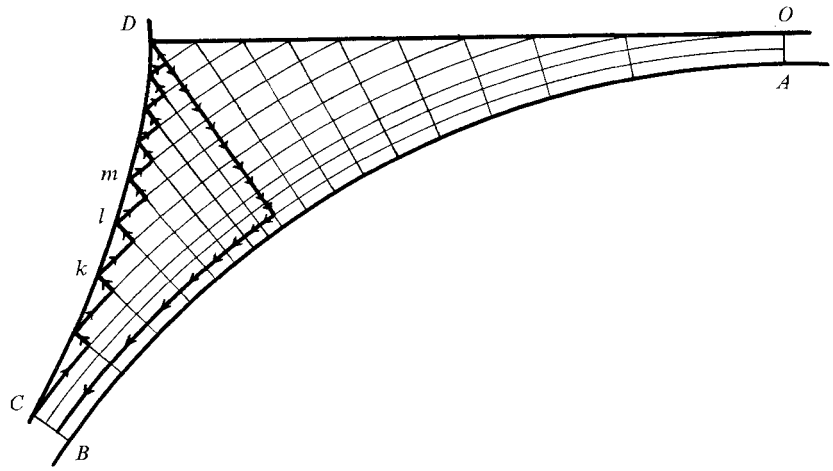

FIGURE 7. Typical finite-difference mesh. The heavy line shows the path followed in determining the pressure ratio at nodes on the tape, or roller, boundary and on the shear-free boundary CD.

3. Outline of the numerical method and comparison with experimental results

3.1. *Numerical method*

In the numerical analysis dimensionless ratios are used. In developing the theory, however, it is more convenient to use dimensional quantities. The numerical scheme is adapted from a procedure used by Griffin & Varga (1963) for the solution of plane elasticity problems. A polar mesh, origin at the guide centre, is imposed on $OABCD$ in the manner shown in figure 7. The intersections of the mesh lines and the boundary coincide with mesh nodes. As boundary CD is altered during a solution the mesh is also altered and the number of nodes remains constant. A first-order finite-difference equation in terms of the stream function is obtained at each node by Taylor series expansion or the method described by Griffin & Varga. At a regular node in which the boundary conditions do not explicitly affect the equation, see figure 8,

$$f_{01}(\nabla^2\psi)_1+f_{02}(\nabla^2\psi)_2+f_{03}(\nabla^2\psi)_3+f_{04}(\nabla^2\psi)_4-(f_{01}+f_{02}+f_{03}+f_{04})(\nabla^2\psi)_0=0, \quad (3.1)$$

where
$$f_{01}=-(r_2-r_4)/2r_0(\theta_1-\theta_0), \qquad f_{02}=(r_0+r_2)(\theta_3-\theta_1)/4(r_2-r_0)$$
$$f_{03}=-(r_4-r_2)/2r_0(\theta_3-\theta_1), \qquad f_{04}=(r_0+r_4)(\theta_1-\theta_3)/4(r_4-r_0),$$
$$(\nabla^2\psi)_0=A_0^{-1}[f_{01}\psi_1+f_{02}\psi_2+f_{03}\psi_3+f_{04}\psi_4-(f_{01}+f_{02}+f_{03}+f_{04})\psi_0] \quad (3.2)$$

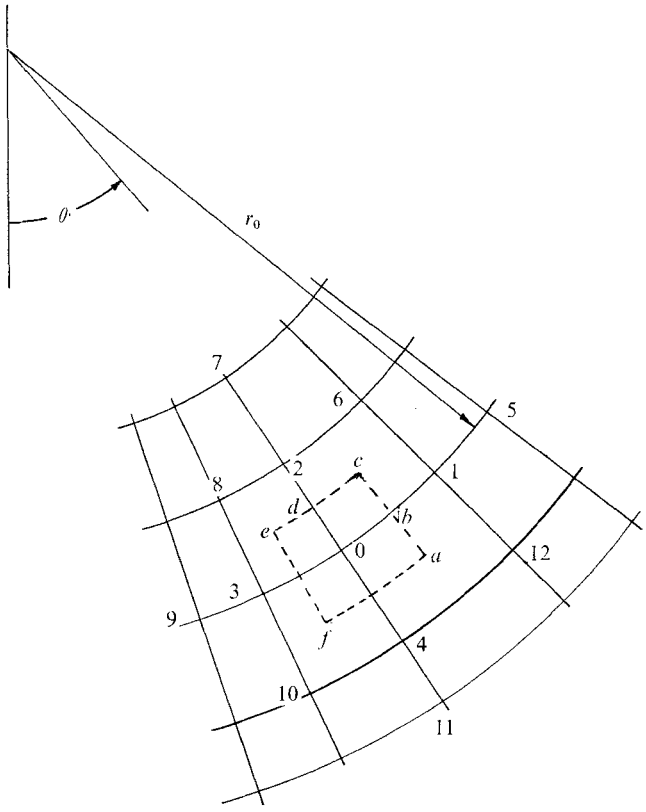

FIGURE 8. Detailed view of mesh.

and $$A_0 = \tfrac{1}{16}(r_4+2r_0+r_2)(r_4-r_2)(\theta_1-\theta_3),$$

with similar expressions for $(\nabla^2\psi)_i, i = 1,2,3,4$. ($A_0$ is the area of the dashed figure *acef*.) To describe the use of equations (3.1) and (3.2) let the finite-difference equation for the typical node 0 be written

$$\sum_{i=0}^{12} a_i\psi_i = 0. \tag{3.3}$$

Node 1 is tested to determine whether it lies on a boundary. If it does, the appropriate boundary conditions are introduced (see below); if not the four nodes surrounding it, used in determining the finite-difference expression for $(\nabla^2\psi)_1$, are tested similarly. If any do lie on the boundary the corresponding term in (3.3) is known since ψ is known on each boundary. The corresponding term in (3.3) is therefore known and is moved to the right-hand side. For those nodes that do not lie on the boundary the contribution to each coefficient a_i from $(\nabla^2\psi)_1$ is determined. Then, in turn, nodes 2, 3 and 4 are similarly treated.

At the boundaries ψ and $\nabla^2\psi$ are prescribed. On OA, BC, and DO these are known from §2.4. On AB, the guide boundary,

$$(\nabla^2\psi)_i = \frac{2}{h_{ij}^2}(\psi_j + Uh_\infty) - 2\frac{U}{h_{ij}} + \frac{U}{R}, \tag{3.4}$$

where i denotes a node on the boundary AB, j is the adjacent internal node along the radial line through i, and h_{ij} is the distance between nodes i and j. On the shear-free boundary CD, as is proved in the appendix,

$$\nabla^2\psi = -2\kappa\,\partial\psi/\partial n, \tag{3.5}$$

where $$\frac{\partial\psi}{\partial n} = \frac{\partial\psi}{\partial r}\cos\delta + \frac{1}{r}\frac{\partial\psi}{\partial\theta}\sin\delta \tag{3.6}$$

and δ is the angle between the outward normal n to CD at a node and the radial mesh line through the node, see figure 7. First-order finite-difference expressions are then substituted for $\partial\psi/\partial r$ and $\partial\psi/\partial\theta$. The values of κ and δ are obtained from the polynomial expression for CD. With the above results a finite-difference equation is obtained for each internal mesh node. With the mesh used, shown in figure 7, there are 96 equations.

The solution for the stream function at the mesh nodes is found by matrix inversion (as performed at the Stanford Computing Center 1969). The value of $\nabla^2\psi$ is now obtained from (3.2) for internal nodes and from the appropriate boundary condition for boundary nodes. The difference in pressure between any adjacent nodes can be calculated from the harmonic conjugate relations between $\nabla^2\psi$ and p/μ. In figure 8, consider that p/μ is known at node 0 and to be found at node 1. On the line 204, $\nabla^2\psi$ is 'fitted' to the quadratic expression

$$\nabla^2\psi = b_1 + b_2 r + b_3 r^2. \tag{3.7}$$

At node 0 then $$\partial(\nabla^2\psi)/\partial r = b_2 + 2b_3 r.$$

A similar procedure is used to determine $\partial(\nabla^2\psi)/\partial r$ at node 1. On the arc 01, p/μ is approximated by the quadratic expression

$$p/\mu = c_1 + c_2\theta + c_3\theta^2, \tag{3.8}$$

where the coefficients c_i are evaluated for (3.8) applied at node 0, and

$$\frac{1}{r}\frac{\partial(p/\mu)}{\partial\theta} = \frac{\partial(\nabla^2\psi)}{\partial r} \tag{3.9}$$

is applied at nodes 0 and 1. Thus p/μ at node 1 is found. Moving as indicated in figure 6, p/μ is evaluated at each mesh node on the path starting and ending at section BC, along which the pressure is uniform. The accumulated error may then be determined. This was generally found to be approximately 2% of the maximum value of pressure on the path. To eliminate the difference between the initial and final values p/μ is corrected by the same 'error per step'.

To determine the normal stress on boundary CD the normal strain rate must be found. It is proved in the appendix that

$$\dot{\epsilon}_n = -\frac{\partial}{\partial s}\left(\frac{\partial\psi}{\partial n}\right), \tag{3.10}$$

where s is the distance along boundary CD, increasing in the direction from D to C. To determine $\dot{\epsilon}_n$ at node l on CD in figure 7, $\partial\psi/\partial n$ is determined at k, l, and m from equation (3.6), where $\partial\psi/\partial r$ and $\partial\psi/\partial\theta$ are obtained by quadratic fitting. The distance along boundary CD between nodes may be obtained from the polynomial expression for CD; however, the straight-line approximation was found to give virtually indistinguishable results. The values of $\partial\psi/\partial n$ are 'fitted' to a quadratic expression in s, and $\dot{\epsilon}_n$ is found from (3.10). The normal stress at nodes on CD is then obtained from the constitutive relation, see (2.23), thus completing the solution to the flow problem with the prescribed shear-free boundary.

3.2. *Comparison with experimental results*

The procedure outlined in §3.1 was applied to the separating flow between partially immersed counter-rotating rollers examined by Pitts & Greiller. This served two purposes. A distinctive feature of the observed stable two-dimensional flow is the presence of two eddies under the lowest point of the surface tension membrane. These eddies could be a consequence of inertia effects in the real fluid. A numerical analysis based on the exact slow viscous flow equations, however, shows that this is not so. Second, since there appears to be no analytic solutions or special cases with which to verify the numerical results, the experimental data can serve as a check on the numerical solution.

The flow is indicated in figure 9. In region $OABCD$ the problem is similar to that dealt with in §2. Here, however, the flow rate between the rollers is not known and must be found as part of the solution. For any given flow rate, providing the assumptions of the numerical method are satisfied, a numerical solution in $OABCD$ can be found. This yields a value of the pressure at the nip section. With no exact solution for the flow below the nip, the following widely used procedure is adopted (e.g. Banks & Mills 1954; Taylor 1963). From a Reynolds flow analysis below the nip, in which the roller boundary is replaced by a parabola with a common tangent and radius of curvature at the nip section (see §2.2), the

pressure at the entrance to the narrowing gap between the rollers, p_b say, may be obtained, where

$$p_b = \frac{-(4-3\lambda)\,3\,2^{\frac{1}{2}}\pi}{16}\frac{\mu U}{R}\left(\frac{R}{h_0}\right)^{\frac{3}{2}} + p_0.$$

The value of p_b thus obtained should equal atmospheric pressure taken as zero, gravity effects being disregarded. Figure 10 shows how the dimensionless pressure ratio $pR^2/\mu U h_0$ comes close to the asymptotic value $p_b R^2/\mu U h_0$ while the parabolic approximation for the roller boundary is close to the roller and the Reynolds flow assumption is still valid. By solving several problems for different flow rates for which p_b varies between negative and positive values, the correct flow rate is obtained by interpolation.

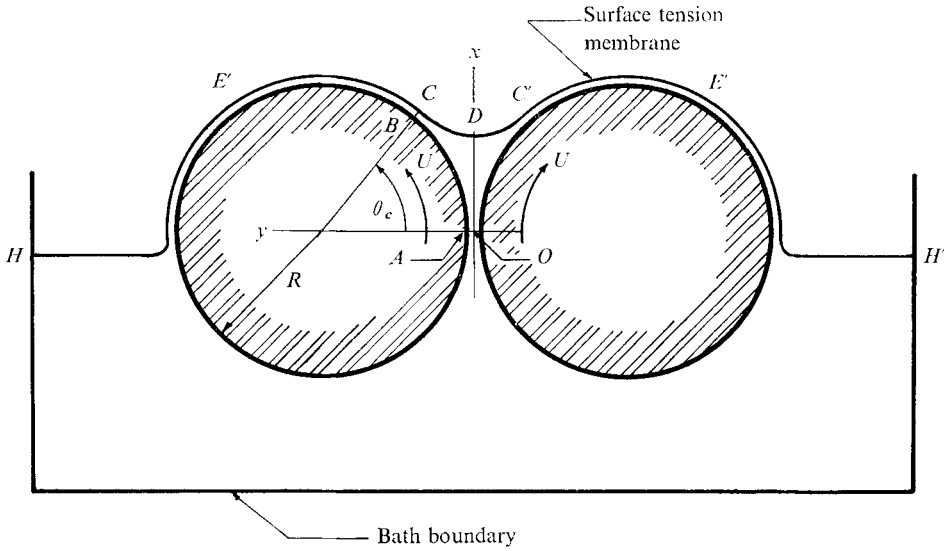

FIGURE 9. The flow examined by Pitts & Greiller.

For the flow of figure 3

$$\lambda = 1{\cdot}380 \quad \text{and} \quad \frac{p_b R^2}{\mu U h_0} = +19{\cdot}13 \times 10^3.$$

With a second flow rate taken as $\lambda = 1{\cdot}340$ it was found that

$$\frac{p_b R^2}{\mu U h_0} = -2{\cdot}48 \times 10^3.$$

From linear interpolation the value of λ corresponding to zero p_0 is $\lambda = 1{\cdot}345$.

In §3 the experimental determination of the flow rate was approximate. The reported results are confined to the mean value and the range of λ for all experiments (with varying h_0/R and $\mu U/T$). These were found to be

$$\text{mean}\,(\lambda) = 1{\cdot}33 \quad \text{and} \quad 1{\cdot}26 \leqslant \lambda \leqslant 1{\cdot}38.$$

A comparison can also be made between the locations of point D, the lowest

point of the meniscus, in the theoretical and experimental results. From data kindly supplied by Dr E. Pitts, with

$$\mu U/T = 0{\cdot}1 \quad \text{and} \quad h_0/R = 0{\cdot}010,$$

x_D/R lies in the range $0{\cdot}28 < x_D/R < 0{\cdot}32.$

The numerical solution yields

$$x_D/R = b_0 = 0{\cdot}330,$$

which is higher than expected, but still close to the experimental values. A qualitative comparison can be made between the theoretical streamline pattern and the sketch of a typical observed streamline pattern, figure 2 of Pitts & Greiller. Corresponding to the eddies observed in the experimental flow there are eddies in the flow of figure 3.

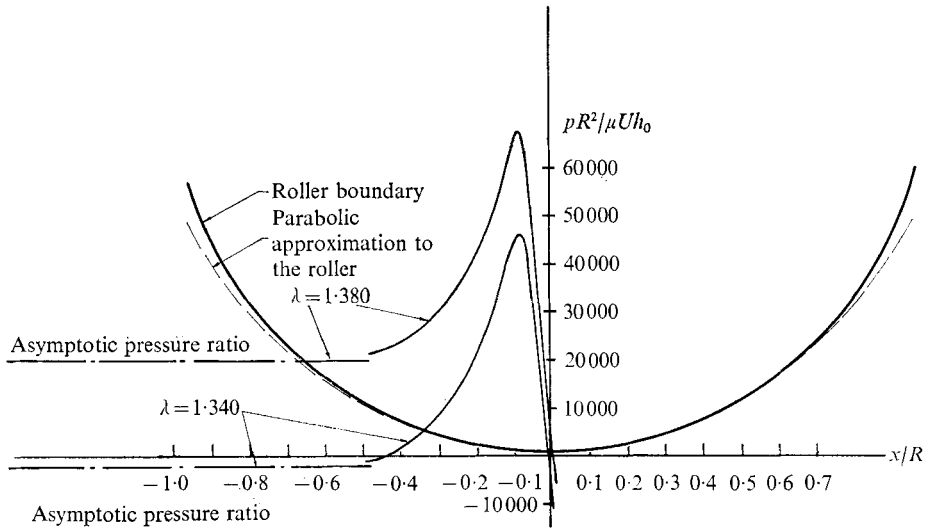

FIGURE 10. The variation of pressure in the region below the nip ($x < 0$) from lubrication theory, for two flow rates. $h_0/R = 0{\cdot}01$.

The author wishes to express his sincere appreciation to the late Dr J.N. Goodier of Stanford University for many stimulating discussions and the encouragement received during the course of this work, also to Dr J.R. Spreiter of Stanford University for help and advice. The support of the U.S. Office of Naval Research is also gratefully acknowledged.

Appendix. Proof of equations (3.5) and (3.10)

In figure 11, CD represents a shear-free streamline. The co-ordinates s and n are, respectively, the distance along CD in the direction indicated, and the outward normal. At any point on CD, e.g. point O, the Cartesian axes locally coincident with s and n are τ and η respectively.

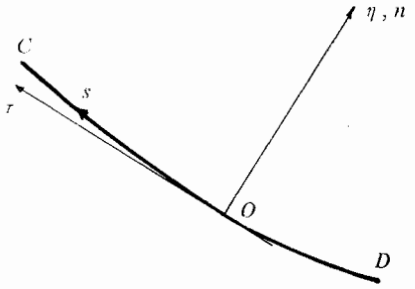

FIGURE 11. The Cartesian co-ordinates τ, η, coincident at point O with the curvilinear system s, n.

At O
$$\frac{1}{\mu}\tau_{ns} = \dot{\gamma}_{ns} = \dot{\gamma}_{\eta\tau} = \frac{\partial u_\eta}{\partial \tau} + \frac{\partial u_\tau}{\partial \eta} = -\frac{\partial^2 \psi}{\partial \tau^2} + \frac{\partial^2 \psi}{\partial \eta^2} = 0,$$

$$\nabla^2 \psi = \frac{\partial^2 \psi}{\partial \tau^2} + \frac{\partial^2 \psi}{\partial \eta^2},$$

where $\dot{\gamma}_{ns}$ and $\dot{\gamma}_{\eta\tau}$ are shear strain rates. Hence, at O

$$\nabla^2 \psi = 2\frac{\partial^2 \psi}{\partial \tau^2} = 2\left(\frac{\partial^2 \psi}{\partial s^2} - \kappa \frac{\partial \psi}{\partial n}\right),$$

where κ is positive when the positive direction of n is on the concave side of CD. Since CD is a streamline

$$\nabla^2 \psi = -2\kappa \partial \psi / \partial n.$$

Clearly the above argument is valid at any point on CD, which thus proves (3.5).

Similarly, at O

$$\dot{\epsilon}_n = \dot{\epsilon}_\eta = \frac{\partial u_\eta}{\partial \eta} = -\frac{\partial}{\partial \tau}\left(\frac{\partial \psi}{\partial \eta}\right) = -\frac{\partial}{\partial s}\left(\frac{\partial \psi}{\partial n}\right) - \kappa \frac{\partial \psi}{\partial s}$$

and, since CD is a streamline, $\dot{\epsilon}_n = -\frac{\partial}{\partial s}\left(\frac{\partial \psi}{\partial n}\right)$.

REFERENCES

BANKS, W. H. & MILLS, C. C. 1954 *Proc. Roy. Soc.* A **223**, 414.
BICKERMAN, J. J. 1968 *The Science of Adhesive Joints*. Academic.
BRETHERTON, F. P. 1961 *J. Fluid Mech.* **10**, 166.
GRIFFIN, D. S. & VARGA, R. S. 1963 *J. Soc. Indust. Appl. Math.* **11**, 4.
LAMB, H. 1932 *Hydrodynamics*. Cambridge University Press.
MCEWAN, A. D. & TAYLOR, G. I. 1966 *J. Fluid Mech.* **26**, 1.
PITTS, E. & GREILLER, J. 1961 *J. Fluid Mech.* **11**, 33.
TAYLOR, G. I. 1963 *J. Fluid Mech.* **16**, 595.